

PSF estimation by gradient descent fit to the ESF

Elisa H. Barney Smith
Boise State University
Boise, Idaho, USA
EBarneySmith@boisestate.edu

ABSTRACT

Calibration of scanners and cameras usually involves measuring the point spread function (PSF). When edge data is used to measure the PSF, the differentiation step amplifies the noise. A parametric fit of the functional form of the edge spread function (ESF) directly to the measured edge data is proposed to eliminate this. Experiments used to test this method show that the Cauchy functional form fits better than the Gaussian or other forms tried. The effect of using a functional form of the PSF that differs from the true PSF is explored by considering bilevel images formed by thresholding. The amount of mismatch seen can be related to the difference between the respective kurtosis factors.

Keywords: Spatial attribute characterization, point spread function, edge spread function, kurtosis factor.

1. INTRODUCTION

To use desktop scanners and cameras in scientific research, it is necessary to carefully calibrate the response of the optics in those systems. An estimate of the actual PSF shape and size usually provides the desired information. Numerous methods for estimating the PSF have been developed over time as researchers have encountered this need. Many of those methods directly estimate the PSF by measuring the response to prespecified inputs to the imaging system.

The most common method of estimating the properties of the optical system is through use of a knife edge. Chazallet and Glasser compared methods of using a sinusoidal input, a bar chart input, and a knife-edge towards the goal of estimating the PSF with particular attention to spatial sampling and concluded that the knife-edge method, which uses a high contrast edge, or a step function in intensity, to produce an ESF was most favorable overall [5]. PSF estimation from a slanted edge has been refined over the years as the applications and the required detail have evolved. Cordella and Nagy used a knife edge and computed the spot size by counting the number of pixels with values in the range between 10% and 90% of the black and white levels [6]. Simonds developed a method that does not depend on the rotational symmetry assumption to estimate the 2-D modulation transfer function (MTF) using a series of knife-edge measurements [18]. Wong analyzed how the misalignment of a knife-edge from the sensor elements affects the MTF [20]. Reichenbach et al. describe an “extended knife-edge technique” for MTF estimation where they use the fact that the edge is not perfectly aligned with the columns of the sensor elements to extend the accuracy beyond the Nyquist frequency of the digital sensor. This, through the Vernier scale principle, leaves extra sample points available for averaging to reduce the effects of noise [16]. Reichenbach’s approach specifically considers the effects of the spatial quantization in the characterization of the image acquisition system. This method was then incorporated into the ISO Standard 12233 [11]. Burns investigated the influence of several variables in the estimation process on bias and variation of the estimates and suggested refinements to improve location of the edge and estimation of the slope [2, 3].

Researchers often take the measured knife edge data, perform a derivative or differencing operation and fit it to a functional form to get an estimate of the PSF or line spread function (LSF). The noise in the scanned image is amplified by the differentiation step needed to convert the observed ESF to a PSF. This can obscure the true PSF shape. Smith proposed a method of directly fitting a Hermite polynomial to the measurements of the ESF. Then by knowing the relation between the coefficients of the Hermite polynomial and a parametric form representing the MTF, the MTF can be directly reached [19]. This paper expands on the Smith’s idea of doing a parametric fit to the ESF, but restricts the form to a common function instead of a Hermite polynomial. This can still be applied to multiple rows of edges combined through Reichenbach’s method to represent the shape of the ESF with more samples to reduce the effects of noise, but by directly fitting the functional form of the PSF to the data, the effect of differentiation on the raw data is eliminated.

In this paper the PSF is specified parametrically under five different PSF(LSF)/ESF functional form assumptions: square

Table 1: PSF and ESF Equations

Functional Form	PSF(x;w)	ESF(x;w)
Square Pulse	$\frac{1}{w_S} \quad -\frac{w_S}{2} < x < \frac{w_S}{2}$ $0 \quad \textit{else}$	$0 \quad x \leq -\frac{w_S}{2}$ $\frac{1}{w_S}x + \frac{1}{2} \quad -\frac{w_S}{2} < x \leq \frac{w_S}{2}$ $1 \quad x > \frac{w_S}{2}$
Triangular Pulse	$4\frac{x}{w_T} + \frac{2}{w_T} \quad -\frac{w_T}{2} < x < 0$ $-4\frac{x}{w_T} + \frac{2}{w_T} \quad 0 \leq x < \frac{w_T}{2}$ $0 \quad \textit{else}$	$0 \quad x \leq -\frac{w_T}{2}$ $2\left(\frac{x}{w_T} + \frac{1}{2}\right)^2 \quad -\frac{w_T}{2} < x \leq 0$ $1 - 2\left(\frac{x}{w_T} - \frac{1}{2}\right)^2 \quad 0 < x \leq \frac{w_T}{2}$ $1 \quad x > \frac{w_T}{2}$
Raised Cosine	$\frac{1}{w_C} \left(1 + \cos\left(2\pi\frac{x}{w_C}\right)\right)$	$0 \quad x \leq -\frac{w_C}{2}$ $\frac{x}{w_C} + \frac{1}{2} + \frac{1}{2\pi} \sin\left(2\pi\frac{x}{w_C}\right) \quad -\frac{w_C}{2} < x \leq \frac{w_C}{2}$ $1 \quad x > \frac{w_C}{2}$
Gaussian	$\frac{1}{\sqrt{2\pi}\sigma} e^{-\frac{1}{2}\left(\frac{x}{\sigma}\right)^2}$	$\textit{erf}\left(\frac{x}{\sigma}\right) + \frac{1}{2}$
Cauchy	$\frac{\alpha/\pi}{x^2 + \alpha^2}$	$\frac{1}{\pi} \textit{atan}\left(\frac{x}{\alpha}\right) + \frac{1}{2}$

pulse, triangular pulse, raised cosine, Gaussian and Cauchy. The formulas used for each are shown in Table 1. Each PSF also has a parametric ESF. Each of these ESFs will be fit by gradient descent to the individual rows to minimize the error

$$\textit{error} = \sum_i [\textit{esf}(x(i), \mu, w, a, b) - \textit{data}(x(i))]^2 . \quad (1)$$

This estimates the edge location, μ , to sub-pixel accuracy, while also calculating the best width parameter, w , and the a and b reflectance levels. A line is fit through estimates of the edge locations over multiple rows by linear regression to improve their accuracy. These edge locations are then used to get a better estimate of the knife edge location used to combine the multiple rows of data to get a composite ESF. The ESF parameters are then estimated from this composite edge, again by gradient descent, to minimize the error shown in Equation 1.

While the paper is assumed to be totally white and the ink is assumed to be totally black, even after conversion of the gray level intensities to reflectances, this is rarely the case. This discrepancy can not be ignored. Parameters a and b were included in the estimation process to ‘stretch’ the ESF to fit the actual intensity ranges set by the reflectance of the paper and ink.

Experiments using this proposed method of estimating from the ESF form will be shown in the next section, followed by an analysis of how the magnitude of the mis-fit between functional forms can be predicted by looking at the kurtosis

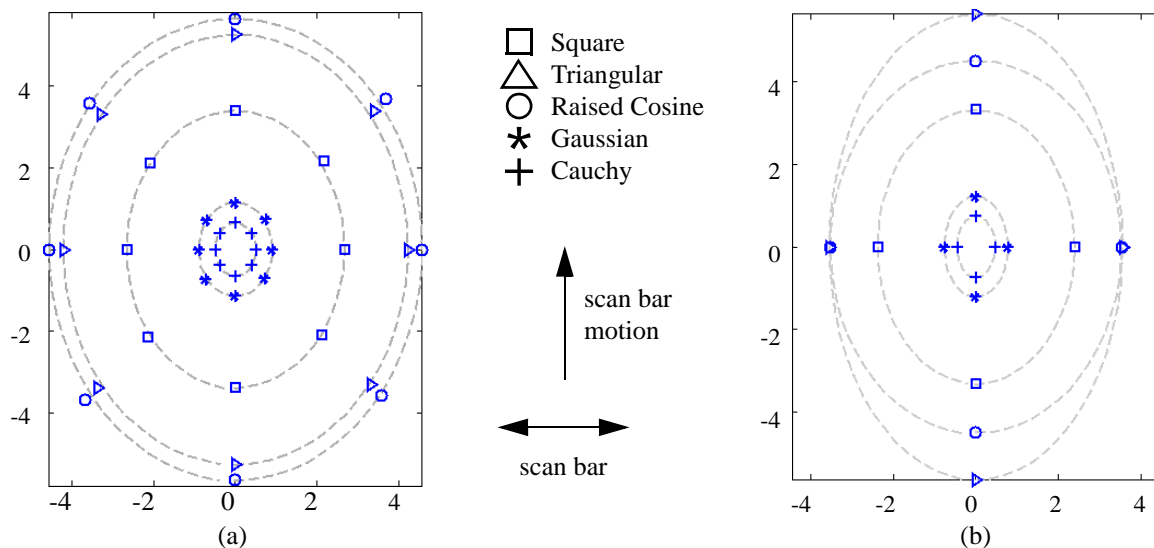


Figure 1: Plot of PSF width estimates (a) at four angles on the HP Scanjet 4c and (b) at two angles on the Apple Color One. Estimates for five shape hypotheses are shown. The PSF is not circularly symmetric for either scanner.

factors of the assumed PSF and the actual PSF.

2. PSF ESTIMATION EXPERIMENTS

This section describes the experiments and corresponding results of measuring the PSF from grey-level information. The scanning experiments were done using two scanners, an HP Scanjet 4c and an Apple Color One Scanner. The HP Scanjet 4C is a 600dpi optical resolution color scanner. The Apple scanner has 300dpi optical resolution. The two scanners allow testing of the algorithms under different optical resolutions and potentially different PSF shapes. Both scanners were used to scan test charts in grey-tone mode to produce 8-bit deep images. A mapping derived from a scan of the reflectance step charts in [12] was used to convert the 8-bit gray level values into reflectance. A knife edge image was scanned and converted to reflectance units on both the ScanJet and the Apple Color One scanners. The ESF corresponding to five of the proposed PSF shapes were fit to the edge scans.

The PSF widths were measured at four different orientations in the HP scanner to determine whether the PSF is circularly symmetric: in the direction of the array sensor, in the direction of the motion of the scanning bar, and at ± 45 degrees to the array sensor. The width estimates differed by 20% between the widths along the scan bar and in the direction of scan bar motion. Thus, the PSF does not have circular symmetry in two dimensions. Plots of the width estimates by angle, including the widths estimated at $\pm 45^\circ$ with an ellipse fit to the estimates for all five reflectance PSF shape hypotheses, are shown in Figure 1a. Figure 1b shows graphically the estimates for the Apple Color One scanner in the direction of the array sensor and in the direction of the motion of the scanning bar also with ellipses fit to the data. The PSF for the Apple scanner is more elliptical than the PSF for the HP scanner. This distortion can actually be seen in images scanned on the Apple scanner.

Figure 2 shows the ESF for the best fit parameters compared with the composite ESF. Tables 2 and 3 show the estimates of the PSF width parameters resulting for each PSF assumption at each angle for the HP scanner and the Apple Color One scanner respectively. While there is good fit to all forms including the Gaussian, the best fit on both scanners was the Cauchy. The edge resulting on the Apple One scanner (not shown) does not make a good match for any PSF other than the Cauchy. The estimation was more difficult on the Apple scanner because the response to the white was still changing at a larger radius than the response to the black. This particularly affected the estimate for the raised cosine along the scan bar direction making it appear anomalous compared to the other estimates in Figure 1. This level in fit among different PSF functional forms was evaluated subjectively and quantified by comparing the mean square error (MSE) of the fits shown in the tables. The Cauchy function fits the best both graphically and numerically with the MSE being one half to one third the size of the MSE for the best fit to a Gaussian. Note that the MSE numbers should not be compared across orientations as different numbers and lengths of rows were used for different scans.

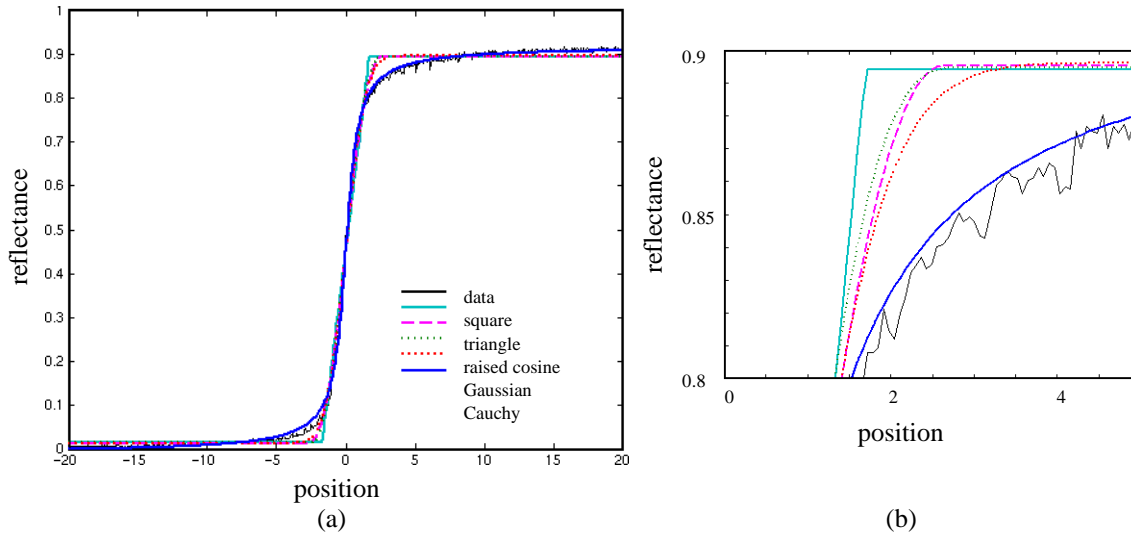


Figure 2: (a) Plot of composite knife edge from the HP Scanjet 4c. Best fit ESF for five different shape hypotheses are shown. (b) Close up of the knee of the plot.

Table 2: PSF width estimates from grey level knife edge on the HP ScanJet scanner.

PSF Shape Assumption	Along Sensor Row		Scan Bar Motion Direction	
	Width Estimate	MSE	Width Estimate	MSE
Square	$w_S=2.67$	0.30	$w_S=3.39$	0.31
Triangular	$w_T=4.22$	0.22	$w_T=5.26$	0.19
Raised Cosine	$w_C=4.57$	0.22	$w_C=5.65$	0.20
Gaussian	$\sigma=0.90$	0.19	$\sigma=1.14$	0.17
Cauchy	$\alpha=0.50$	0.06	$\alpha=0.65$	0.04
PSF Shape Assumption	Diagonal -45 degrees		Diagonal 45 degrees	
	Width Estimate	MSE	Width Estimate	MSE
Square	$w_S=2.96$	1.31	$w_S=3.05$	1.20
Triangular	$w_T=4.68$	0.97	$w_T=4.80$	0.81
Raised Cosine	$w_C=5.05$	1.00	$w_C=5.23$	0.72
Gaussian	$\sigma=1.01$	0.88	$\sigma=1.04$	0.84
Cauchy	$\alpha=0.55$	0.35	$\alpha=0.55$	0.35

3. KURTOSIS

For many applications the level of the fit to the PSF is not significant, but for other applications, errors in the fit have a large effect. One application for which the information about the PSF is needed is in modeling scanners for document image analysis. Here the PSF width together with the binarization threshold jointly affect the resulting character image quality. Broad correlation with the actual PSF shape will allow the general shape of the degraded character to be predicted, but a more exact fit is needed when evaluating the types of degradations character images incur when being scanned. The degradations that appear in character images are more noticeable when the threshold is either very high (near 0.9 reflectance) or very low (near 0.1 reflectance). This is exactly the region where the incorrect functional form of

Table 3: PSF width estimates from grey level knife edge on the Apple Color One scanner

PSF Shape Assumption	Along Sensor Row		Scan Bar Motion Direction	
	Width Estimate	MSE	Width Estimate	MSE
Square	$w_S=2.39$	1.07	$w_S=3.32$	1.41
Triangular	$w_T=3.56$	0.91	$w_T=5.65$	1.17
Raised Cosine	$w_C=3.53$	0.94	$w_C=4.51$	1.39
Gaussian	$\sigma=0.77$	0.87	$\sigma=1.22$	1.10
Cauchy	$\alpha=0.46$	0.51	$\alpha=0.74$	0.45

Table 4: Kurtosis factors.

Distribution	Kurtosis Factor
Square Pulse (Uniform)	1.78
Triangular Pulse	2.40
Raised Cosine	2.41
Gaussian	3.00
Cauchy	undefined, but large

the PSF/ESF is most noticeable. How the edges of characters and line drawings are distorted is a function of the ESF. PSFs where the tails rapidly decay will have a much smaller edge spread at extreme threshold than PSFs with the same standard deviation but with a heavier tail. The heaviness of the tails in the PSF can be quantified by the kurtosis. The *kurtosis factor* is the ratio of the fourth central moment to square of second central moment.

$$\frac{E\{(x-\mu)^4\}}{E\{(x-\mu)^2\}^2} \quad (2)$$

and is independent of the parameters defining the distribution for many distributions. The kurtosis factors for the 1-D PSF shapes used in this paper are shown in Table 4.

The mismatch between the assumed PSF functional form and the true PSF functional form can be seen in images produced by bilevel systems. The effect of the mismatch can be quantified by the difference in the kurtosis factor. Systems where the kurtosis factor for the assumed functional form is smaller than the kurtosis factor of the true PSF functional form will have edges spread less far than expected and vice versa. This is illustrated in two experiments. First, synthetic characters were created with a PSF of each of the forms shown in Table 4 and using PSF widths that are the average of the values in Table 2 for horizontal and vertical directions. These were then thresholded at a thresholds of $\Theta=0.1, 0.3$ and 0.5 . If the shape of the PSF is insignificant, these characters, shown in Figure 3 at 4x their original size, should be identical since all PSF widths are those estimated from the same knife edge in Section 2. Visually the characters made with the same thresholds appear quite similar. The Hamming distance between every pair of these characters at common threshold values was calculated. The results are shown in Table 5. Notice that as the kurtosis factor difference increases, that the Hamming distance is generally greater. When looking at the Hamming distances that result when the threshold is increased, the Hamming distances get smaller. At a threshold of $\Theta=0.5$, the effect of the tail of the ESF should be at its minimum. It is certainly smaller than at other thresholds. This illustrates how when models of optical systems are being used for bilevel analysis and the functional form of the PSF doesn't match the PSF of a real system, predicted results would be different than expected.

The second experiment to illustrate this shows the effect of measuring the PSF width from a bilevel image when the PSF form is incorrectly assumed. Methods have been developed [1] to estimate the PSF width and binarization threshold from bilevel scans of a star sector test chart such as found in the Kodak Digital Science Imaging Test Chart TL-5003 [12]. This experiment was run by blurring a synthetically generated star chart with one PSF and thresholding it at 9 different thresh-

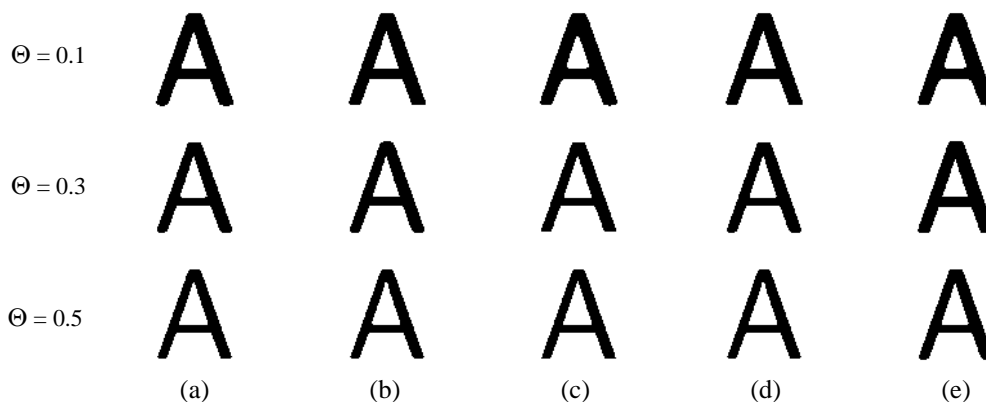


Figure 3: Images of characters created with PSFs of the functional form and widths (a) square pillbox, $w_S = 3.03$, (b) triangular (conical), $w_T = 4.74$, (c) raised cosine, $w_C = 5.11$, (d) bivariate Gaussian, $\sigma = 1.02$, and (e) Cauchy, $\alpha = 0.575$. Row 1 was made at a threshold of $\Theta = 0.1$, row 2 at $\Theta = 0.3$, and row 3 at $\Theta = 0.5$.

Table 5: Hamming distance between characters with “same” PSF width but different functional forms over three threshold values.

	Threshold, $\Theta=0.1$					Threshold, $\Theta=0.3$					Threshold, $\Theta=0.5$				
	S	T	RC	G	C	S	T	RC	G	C	S	T	RC	G	C
Square	0	17	0	44	94	0	42	44	39	88	0	2	2	8	27
Triangular	17	0	17	31	79	42	0	2	9	48	2	0	0	6	25
Raised Cos	0	17	0	44	94	44	2	0	11	96	2	0	0	6	25
Gaussian	44	31	44	0	66	39	9	11	0	55	8	6	6	0	21
Cauchy	94	79	94	66	0	88	48	96	55	0	27	25	25	21	0

olds. This was then used as the source data for PSF estimation under five different PSF functional form assumptions. Figures 4, 5, and 6 show the results for five PSF forms when the actual PSF is square, Gaussian and truncated Cauchy respectively. For a given scanner, the PSF width should remain constant for all thresholds used on that scanner. But since the effective ESF is different at different thresholds, when the PSF form doesn't match the actual PSF form, the mismatch will affect the images and thus the estimates. Looking at the square case in Figure 4, the results show that for every estimate based on a PSF with a higher kurtosis factor (i.e., with any other PSF assumptions), when $|\Theta-1/2|$ is large, the estimated PSF width is biased as too small, and when $|\Theta-1/2|$ is small, the estimate is biased as too large. This type of bias is called “right bias”, because when multiple thresholds are shown, they look like a right parentheses “)”. The estimates made under the square PSF assumption are slightly biased the opposite direction (“left bias”) even though the square pillbox was the true PSF. The multiple orientations of the edges in the image relative to the PSF edge make the effective PSF almost cylindrical (cylindrical with a small skirt) which gives the true PSF a slightly higher kurtosis factor than the kurtosis factor used in the estimation procedure (a cylinder has a kurtosis factor of 2, the square pulse has a kurtosis factor of 1.78).

When the PSF used in blurring is a Gaussian, Figure 5, the estimates made based on a PSF with a higher than actual kurtosis factor (Cauchy) are again “right biased” such that when $|\Theta-1/2|$ is large, the PSF width is underestimated, and when $|\Theta-1/2|$ is small, it is overestimated. When the assumed PSF has a smaller than actual kurtosis factor (square, triangle, raised cosine), the “left bias” is observed so that when $|\Theta-1/2|$ is large, the PSF width is overestimated, and when $|\Theta-1/2|$ is small, it is underestimated. Even though there is bias in the width estimates, because the kurtosis factors of the triangle, raised cosine and Gaussian are close, the bias there is not nearly so pronounced, whereas the differences in kurtosis factors between the Gaussian versus Cauchy and the Gaussian versus the square pulse are greater and thus produce larger distortions. The Cauchy has a very high kurtosis factor. Figure 6 shows that estimates from a star blurred

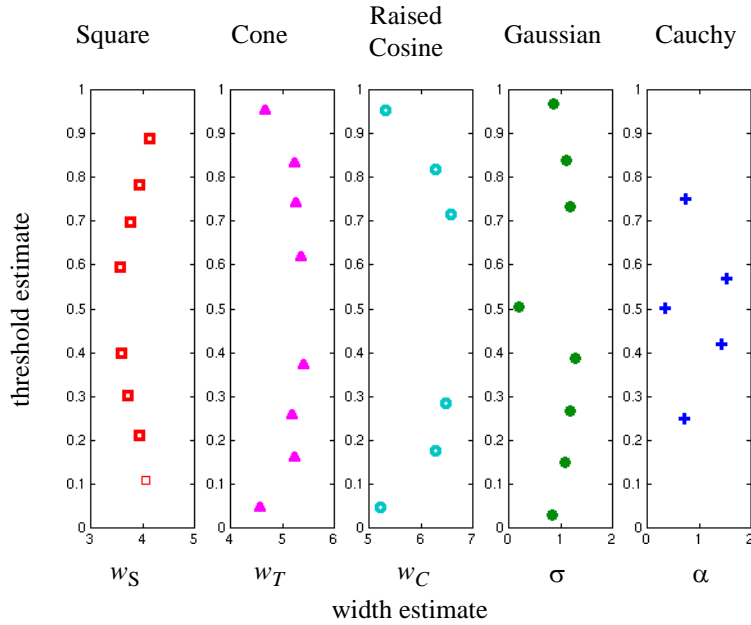


Figure 4: A synthetic star target blurred with a square pillbox PSF, $w_{S2}=4$, produced these estimates under the sector merge method when the indicated PSF assumptions are used.

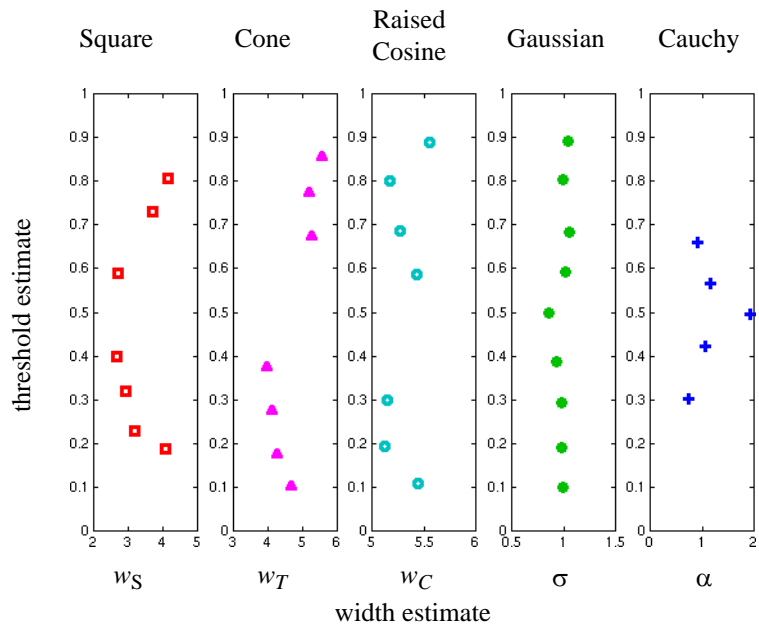


Figure 5: A synthetic star target blurred with a Gaussian PSF, $\sigma=1$, produced these estimates under the sector merge method when the indicated PSF assumptions are used.

with a Cauchy PSF will result in estimates that are significantly “left biased” under all other PSF assumptions.

4. CONCLUSION

A modification of the knife edge method is proposed for estimating the characteristics of a scanner or camera system. It is particularly useful when the data will eventually be used to estimate the camera characteristics in a parametric form. The

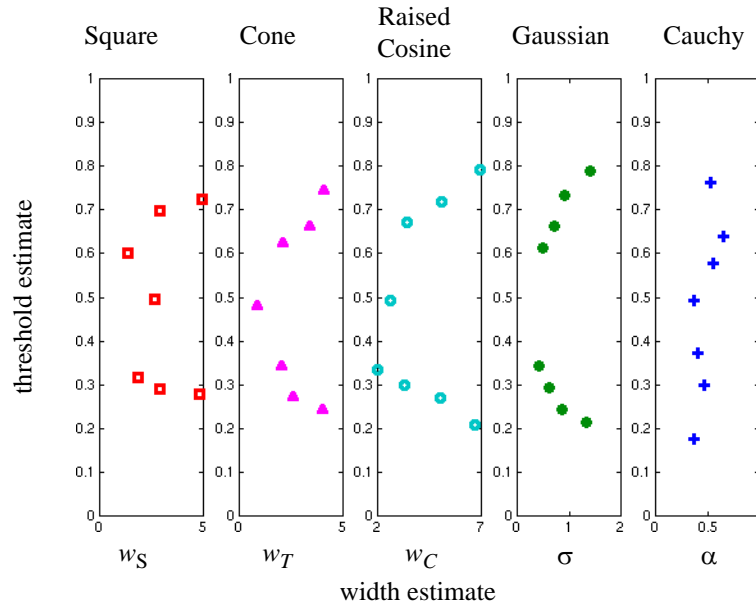


Figure 6: A synthetic star target blurred with a truncated Cauchy PSF, $\alpha=0.5$, produced these estimates under the sector merge method when the indicated PSF assumptions are used.

functional form found to best fit the data from actual scanners was Cauchy. While some researchers [9, 16, 17, 20] have advocated for Cauchy, many researchers prefer to use Gaussian due to other properties of the Gaussian functional form. In bilevel systems assumptions of Gaussian over Cauchy can have effects that alter the assumed form of the image significantly. Similar effects will be seen in gray level systems but they will appear as changes in the very brightest and very darkest gray levels which often can not be discerned by viewers. Researchers can use these descriptions to decide how the assumption of PSF functional form will affect their research.

5. REFERENCES

1. E. H. Barney Smith, "Scanner Parameter Estimation Using Bilevel Scans of Star Charts," Proc. International Conference on Document Analysis and Recognition 2001, Seattle, WA, 10-13 September 2001, pp. 1164-1168.
2. P. D. Burns, "Slanted-Edge MTF for Digital Camera and Scanner Analysis," Proc. Society for Imaging Science and Technology: Image Processing, Image Quality, Image Capture, Systems (PICS) Conference, Portland, OR, March 26-29, 2000, pp. 135-138.
3. P. D. Burns and D. Williams, "Refined Slanted-Edge Measurement for Practical Camera and Scanner Testing," Proc. Society for Imaging Science and Technology: Image Processing, Image Quality, Image Capture, Systems (PICS) Conference, Portland, OR, April 7-10, 2002, pp. 191-195.
4. M. Chang, A. M. Tekalp, A. T. Erdem, "Blur Identification using the Bispectrum," IEEE Trans. Signal Processing, Vol. 39, October 1991, pp. 2323-2325.
5. F. Chazallet, J. Glasser, "Theoretical bases and measurements of the MTF of integrated image sensors," Proc. SPIE Image Quality: An Overview, Vol. 549, Arlington, VA, 9-10 April 1985, pp. 131-144.
6. L. P. Cordella and G. Nagy, "Quantitative Functional Characterization of an Image Digitization System," 6th International Conference on Pattern Recognition, Munich, Germany, 19-22 October 1982, pp. 535-537.
7. W. J. Dallas, H. H. Barrett, R. E. Wagner, C. N. West, "Finite-length line spread function," Journal of the Optical Society of America, Vol. 4, No. 11, November 1987, pp. 2039-2044.
8. D. B. Gennery, "Determination of Optical transfer function by inspection of the frequency domain plot," Journal of the Optical Society of America, Vol. 63, No. 12, December 1973, pp. 1571-1577.
9. C. A. Glasbey, G. W. Horgan, D. Hitchcock, "A note on the grey-scale response and sampling properties of a desktop scanner," Pattern Recognition Letters, Vol. 15, No. 7, 1994, pp. 705-711.
10. H. S. Hou, "Digital Document Processing," John Wiley & Sons, NY, 1983, pp. 307-308.

11. International Standard ISO 12233, Photography - Electronic still-picture cameras - Resolution measurements, 2000.
12. Kodak Digital Science Imaging Test Chart TL-5003, Rev. 1.1, printed 01.20.98, (c) 1995.
13. I. Limansky, "A new resolution chart for imaging systems," *The Electronic Engineer*, June 1968, p. 50.
14. E. W. Marchard, "Derivation of the point spread function from the line spread function," *Journal of the Optical Society of America*, Vol. 54, 1964, pp. 915-919.
15. E. W. Marchard, "From the Line to Point Spread Function: The general case," *Journal of the Optical Society of America*, Vol. 55, 1965, pp. 352-354.
16. S. E. Reichenbach, S. K. Park, R. Narayanswamy, "Characterizing digital image acquisition devices," *Optical Engineering*, Vol. 30, No. 2, March 1991, pp. 170-177.
17. M. Sensiper, G. D. Boreman, A. D. Ducharme, and D. R. Snyder, "Modulation transfer function of detector arrays," *Optical Engineering*, Vol. 32, No. 2, 1993, pp. 395-400.
18. R. M. Simonds, "Two-dimensional modulation transfer functions of image scanning systems," *Applied Optics*, Vol. 20, No. 4, February 1981, pp. 619-622.
19. P. L. Smith, "New Technique for Estimating the MTF of an Imaging System from its Edge Response," *Applied Optics*, Vol. 11, No. 6, June 1972, pp. 1424-1425.
20. H. Wong, "Effect of knife-edge skew on modulation transfer function measurements of charged couple device imagers employing a scanning knife edge," *Optical Engineering*, Vol. 30, No. 9, 1991, pp. 1394-1398.
21. S. H. Zisk and N. Wittels, "Camera Edge Response," *Proc. SPIE symposium on Optics, Illumination, and Image Sensing for Machine Vision II*, Vol. 850, Cambridge, MA, 5-6 November 1987, pp. 9-16.